PERGAMON

Applied Thermal Engineering 22 (2002) 1347–1367

APPLIED THERMAL ENGINEERING

www.elsevier.com/locate/apthermeng

Performance comparisons of desiccant wheels for air dehumidification and enthalpy recovery

L.Z. Zhang *, J.L. Niu

Department of Building Services Engineering, The Hong Kong Polytechnic University, Kowloon, Hong Kong, China

Received 3 October 2001; received in revised form 13 March 2002; accepted 14 March 2002

Abstract

Desiccant wheels have two major applications: air dehumidification and enthalpy recovery. Since the operating conditions are different, heat and mass transfer behaviors in the wheels are quite different. In this paper, the performances of desiccant wheels used in air dehumidification and enthalpy recovery are compared with each other. To accomplish this task, a two-dimensional, dual-diffusion transient heat and mass transfer model which takes into account the heat conduction, the surface and gaseous diffusion in both the axial and the thickness directions is presented. Effects of the rotary speed, the number of transfer units, and the specific area on the performance of the wheel are investigated and compared in the two situations. The cycles that the desiccant and air undergo in the wheel are plotted in psychrometric charts to demonstrate the different heat and moisture transfer mechanisms during the dehumidification and enthalpy recovery processes.

Keywords: Desiccant wheel; Heat and mass transfer; Model; Dehumidification; Enthalpy recovery

1. Introduction

Normally the water vapor content of atmospheric air is small, some tens of grams per kilo of air. Nevertheless, due to the very high heat of vaporization, the latent heat content in air-conditioning is of the same order of the sensible one. The relative importance of latent load increases with the ventilation rates to buildings. Higher ventilation rates are dictated both by better comfort requirement and by the ASHRAE standard 62/1999.

* Corresponding author. Tel.: +852-27665853; fax: +852-27746146.
E-mail address: belzhang@polyu.edu.hk (L.Z. Zhang).

1359-4311/02/$ - see front matter
PII: S1359-4311(02)00050-9

Nomenclature

a	pore radius (m)
A_s	transfer area (m^2)
Bi	Biot number
C	constant in sorption curve
c_p	specific heat ($kJ\,kg^{-1}\,K^{-1}$)
d_e	hydrodynamic diameter of a channel (m)
D_A	combined ordinary and Knudson diffusivity ($m^2\,s^{-1}$)
D_S	surface diffusivity ($m^2\,s^{-1}$)
f	fraction of desiccant in the wheel material
h	convective heat transfer coefficient ($kW\,m^{-2}\,K^{-1}$)
h_m	convective mass transfer coefficient ($kg\,m^{-2}\,s^{-1}$)
H	specific enthalpy ($kJ\,kg^{-1}$)
k	thermal conductivity ($kW\,m^{-1}\,K^{-1}$)
L	length of a channel (m)
Le	Lewis number
M_1	molecular weight ($kg\,kmol^{-1}$)
m_d	mass of the wheel (kg)
$\dot{m}_g$	mass flow rate of air stream ($kg\,s^{-1}$)
N	rotary speed (rpm)
NTU	number of transfer units
P	pressure (Pa)
q_{st}	isosteric adsorption heat ($kJ\,kg^{-1}$)
SDP	specific dehumidification power ($g\,kg^{-1}\,s^{-1}$)
T	temperature (K)
t	time (s)
u_g	velocity of air stream ($m\,s^{-1}$)
V	volume (m^3)
w	water uptake in desiccant (kg water/kg dry desiccant)
w_{max}	maximum water uptake of desiccant ($kg\,kg^{-1}$)
x, y	coordinates (m)

Greek letters

α	angle (rad)
β, λ	coefficients in Eq. (35)
θ	dimensionless temperature
ε	effectiveness
ε_t	total porosity
ϕ	relative humidity
δ	half thickness of channel (m)
ω	moisture content (kg moisture/kg dry air)
ρ	density ($kg\,m^{-3}$)

ζ	tortuosity factor
τ	dimensionless time
ξ	resistance coefficient

Superscripts

*	dimensionless form of the variable

Subscripts

a	air
c	cooling, process stream for dehumidification and exhaust for enthalpy recovery
d	desiccant, dehumidification
g	gas
h	heating, regeneration for dehumidification and process for enthalpy recovery
i	inlet
L	latent
m	moisture
o	outlet
opt	optimum
s	surface, sensible
w	water
x	in x-direction
y	in y-direction

Desiccant wheels have been widely used for air humidity treatment: dehumidification [1–4] and enthalpy recovery [5–7]. In the first case, process air is dried after it flows through the wheel, which rotates continuously between the process air and a hot regenerative air stream. The dried air can either be used directly or be employed to make cooling following further psychrometric processes, i.e. the so-called desiccant cooling. In the latter case, the desiccant wheel rotates between the outside fresh air (process air) and the exhaust air from room. Heat and humidity would be recovered from the exhaust in winter and excess heat and moisture would be transferred to the exhaust to cool and dehumidify the process air in the summer. However, due to different operating conditions, heat and moisture transfer behaves quite differently in the wheels. Regretfully, the performances for air dehumidification and enthalpy recovery have never been systematically compared.

There have been many works in modeling heat and moisture transfer in desiccant wheels. Only considering resistance at the gas–solid interface while neglecting heat conduction and moisture diffusion in the solid, Jurinak and Mitchell [8] and Zheng and Worek [9] used one-dimensional transient models for heat and moisture couplings between the solid desiccant and the air streams in the wheel. The effect of matrix sorption properties was studied in the former case and a full-implicit finite difference technique was employed to obtain the solution in the latter one. As a step forward, San and Hsiau [10] and Simonson and Besant [11] adopted the one-dimensional solid heat conduction equation in their respective models to account for the longitudinal thermal resistance inside the solid. These two studies gave some insight into the heat mass transfer

mechanisms in the desiccant. However, the model of Simonson and Besant neglected the internal moisture resistance in the solid, and that of San and Hsiau considered only the axial surface diffusion resistance by assuming axial surface diffusion as the dominant mass transfer mechanism in the adsorbent.

The model presented here is a dual-diffusion model that takes into account both the heat and the moisture resistance in two dimensions: axial and in-thickness directions of the solid. Moisture transfer is expressed in two forms: surface diffusion and gaseous diffusion (Knudsen and ordinary combined).

2. Mathematical model

2.1. Basic equations

A rotary regenerative desiccant wheel is shown in Fig. 1(a). It is a rotating cylindrical wheel of length L and diameter d_w and it is divided into two sections: adsorption section (angle fraction α_0) and regeneration section (fraction $1-\alpha_0$), where the adsorption and regeneration air streams are in a counter-flow arrangement. The wheel generally consists of a matrix of numerous flow channels which have, depending on the manufacturing process, a rectangular, triangular or sinusoidal shape. The channel walls are parallel to the axis of the wheel, and are made of composite materials which have a desiccant content of $f = 0.7$–0.8.

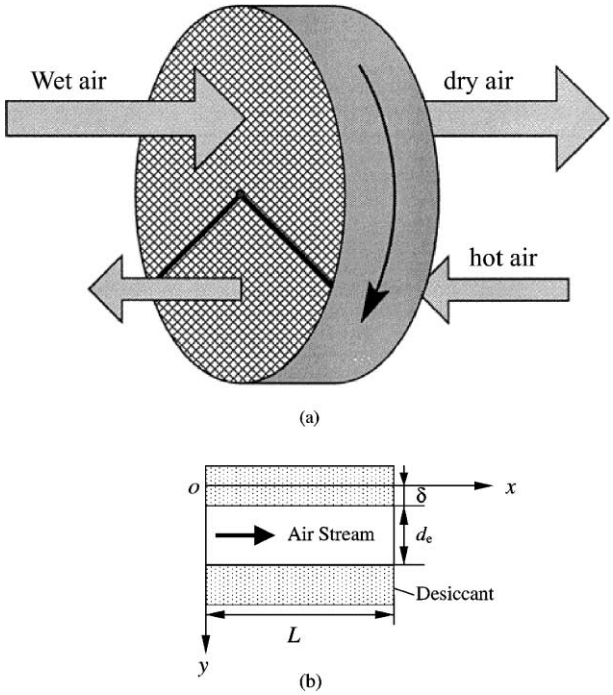

Fig. 1. Schematic of the desiccant wheel showing (a) the entire wheel, (b) a side view of one of the ducts.

For simplicity, some assumptions are made:

(1) One-dimensional air stream flow is considered.
(2) The axial heat conduction and mass diffusion in the fluid are neglected.
(3) No carryover of the fluid in the desiccant wheel is assumed.
(4) The thermodynamic properties in the solid are constants, and uniform.

Consequently, the model used in this study is transient and two-dimensional. Because of symmetry, the mid-plane of a channel can be considered to be adiabatic, and a half-size channel surrounded by dashed line is used as the physical model, as shown in Fig. 1(b).

Heat and mass conservation for the air stream

$$\frac{1}{u_g}\frac{\partial T_g}{\partial t}+\frac{\partial T_g}{\partial x}=\frac{4h}{d_e u_g \rho_g c_{pg}}\left(T_s-T_g\right) \tag{1}$$

$$\frac{1}{u_g}\frac{\partial \omega_g}{\partial t}+\frac{\partial \omega_g}{\partial x}=\frac{4h_m}{d_e u_g \rho_g}\left(\omega_s-\omega_g\right) \tag{2}$$

where u_g is the velocity ($m\,s^{-1}$), T_g and ω_g are temperature (°C) and humidity ratio ($kg\,kg^{-1}$) respectively, t is time (s), x is axial coordinate (m), d_e is the hydrodynamic diameter of the channel (m), ρ_g is the density ($kg\,m^{-3}$) and c_{pg} is the specific heat ($kJ\,kg^{-1}\,K^{-1}$), h and h_m are the convective heat transfer ($kW\,m^{-2}\,K^{-1}$) and mass transfer ($kg\,m^{-2}\,s^{-1}$) coefficients between the air stream and the solid surface, respectively. In the equations, subscripts "s" and "g" refer to "surface" and "gas" respectively. By using heat mass transfer analogy, the relations between h and h_m can be expressed as

$$h_m=\frac{h}{c_{pg}Le} \tag{3}$$

where Le is the Lewis number of air stream.

Boundary conditions

For adsorption section, i.e., $0\leqslant\alpha^*<\alpha_0$:

$$\begin{cases} T_g\big|_{x=0}=T_{ci} \\ \omega_g\big|_{x=0}=\omega_{ci} \end{cases} \tag{4}$$

For desorption section, i.e., $\alpha_0\leqslant\alpha^*<1$:

$$\begin{cases} T_g\big|_{x=L}=T_{hi} \\ \omega_g\big|_{x=L}=\omega_{hi} \end{cases} \tag{5}$$

where subscripts "c", "h", "i" and "o" refer to process air, regenerative air, inlet and outlet, respectively. The dimensionless angle $\alpha^*=\alpha/2\pi$.

Heat conservation in the desiccantz

$$\rho_d c_{tot}\frac{\partial T_d}{\partial t}=k_d\left(\frac{\partial^2 T_d}{\partial x^2}+\frac{\partial^2 T_d}{\partial y^2}\right)+q_{st}\rho_d\frac{\partial w}{\partial t} \tag{6}$$

where ρ_d is the density of dry desiccant ($kg\,m^{-3}$), k_d is the thermal conductivity of the solid ($kW\,m^{-1}\,K^{-1}$), w is the water content in the desiccant ($kg\,kg^{-1}$), q_{st} is the adsorption heat ($kJ\,kg^{-1}$), c_{tot} is the total heat capacity of wet desiccant, which includes two parts: dry desiccant and adsorbed water and is calculated by

$$c_{tot} = c_{pd} + wc_{pw} \tag{7}$$

where c_{pd} and c_{pw} are the specific heats ($kJ\,kg^{-1}\,K^{-1}$) of dry desiccant and liquid water respectively.

Moisture conservation

Two phases of water, namely, gas and adsorbed state, co-exist and diffuse in the pores of the solid. There are three dominant diffusion mechanisms [12]: surface diffusion, ordinary diffusion, and Knudsen diffusion. The first diffusion is in the form of adsorbed state and the latter two are in gas state. If Fick's law is used to express the diffusion dynamics, then the moisture conservation in the solid can be expressed as

$$\varepsilon_t \rho_a \frac{\partial \omega}{\partial t} + \rho_d \frac{\partial w}{\partial t} = \rho_a \left[\frac{\partial}{\partial x}\left(D_A \frac{\partial \omega}{\partial x} \right) + \frac{\partial}{\partial y}\left(D_A \frac{\partial \omega}{\partial y} \right) \right] + \rho_d \left[\frac{\partial}{\partial x}\left(D_S \frac{\partial w}{\partial x} \right) + \frac{\partial}{\partial y}\left(D_S \frac{\partial w}{\partial y} \right) \right] \tag{8}$$

where ε_t is the total porosity of the desiccant. On the right hand side of Eq. (8), the first term is the moisture transfer in gas (combined ordinary and Knudsen diffusion), and the second term is in the adsorbed phase, namely, surface diffusion. D_A and D_S are the effective diffusivities ($m^2\,s^{-1}$) of the combined ordinary and Knudsen diffusion and surface diffusion, respectively. They are calculated by the following equations [12,13].

$$D_A = \frac{\varepsilon_t}{\zeta}\left(\frac{1}{D_{AO}} + \frac{1}{D_{AK}} \right)^{-1} \tag{9}$$

$$D_S = \frac{1}{\zeta} D_0 \exp\left(-0.974 \times 10^{-3} q_{st}/T_d \right) \tag{10}$$

$$D_{AO} = 1.758 \times 10^{-4} \frac{T_d^{1.685}}{P_a} \tag{11}$$

$$D_{AK} = 97a\left(\frac{T_d}{M_1} \right)^{1/2} \tag{12}$$

where ζ is tortuosity factor that accounts for the increase in diffusional length due to the tortuous path of the real pores, D_{AO} is the ordinary diffusivity, D_{AK} is the Knudsen diffusivity, D_0 is a constant for surface diffusion calculation, a is the pore radius of the adsorbent, P_a is the pressure in atmospheres (Pa), T_d is in K, M_1 is the molecule weight of water.

Boundary conditions

$$-k_d \left. \frac{\partial T_d}{\partial y} \right|_{y=\delta} = h\left(T_d - T_g \right) \tag{13}$$

$$\left(-\rho_a D_A \frac{\partial \omega}{\partial y} - \rho_d D_S \frac{\partial w}{\partial y} \right)\Big|_{y=\delta} = h_m(\omega - \omega_g) \tag{14}$$

$$\left.\frac{\partial T_d}{\partial y}\right|_{y=0} = \left.\frac{\partial T_d}{\partial x}\right|_{x=0} = \left.\frac{\partial T_d}{\partial x}\right|_{x=L} = 0 \tag{15}$$

$$\left.\frac{\partial \omega}{\partial y}\right|_{y=0} = \left.\frac{\partial \omega}{\partial x}\right|_{x=0} = \left.\frac{\partial \omega}{\partial x}\right|_{x=L} = 0 \tag{16}$$

where δ is the half thickness of the channel wall (m), and L is the length of the channel (m).

2.2. Normalization of equations

Water content in the desiccant is governed by a general sorption isotherm as

$$w = \frac{f w_{max}}{1 - C + C/\phi} \tag{17}$$

where w_{max} is the maximum water content (kg kg^{-1}), C is a constant that determines the isotherm shape, ϕ is the relative humidity. Selecting T and ω as two independent variables, a differential form of adsorption content can be written in terms of humidity and temperature as

$$dw = \psi\, d\omega + \varphi\, dT \tag{18}$$

where

$$\psi = \left(\frac{\partial w}{\partial \omega}\right)_T \tag{19}$$

$$\varphi = \left(\frac{\partial w}{\partial T}\right)_\omega \tag{20}$$

Using Clapeyron equation to represent the saturation vapor pressure and assuming a standard atmospheric pressure of 101 325 Pa gives the relation between humidity and relative humidity [13] as

$$\frac{\phi}{\omega} = 10^{-6} e^{5294/T} - 1.61\phi \tag{21}$$

where T is in K. The second term on the right side of the equation will generally have less than a 5% effect, thus it can be neglected. Substituting Eqs. (17) and (21) into Eqs. (19) and (20), following equations can be obtained

$$\psi = 10^{-6} e^{5294/T} \frac{f w_{max} C}{(1 - C + C/\phi)^2 \phi^2} \tag{22}$$

$$\varphi = -\frac{5294\phi}{T^2} \frac{f w_{max} C}{(1 - C + C/\phi)^2 \phi^2} \tag{23}$$

where ψ reflects the slope of w to ω, and it is a dimensionless variable. Partial differential φ reflects the slope of w to T, and its unit is K^{-1}. For enthalpy recovery, the bigger the ψ, the better the performance; for air dehumidification, the greater the φ, the better the performance.

Consequently,

$$\frac{\partial w}{\partial t} = \psi \frac{\partial \omega}{\partial t} + \varphi \frac{\partial T}{\partial t} \tag{24}$$

$$\frac{\partial w}{\partial x} = \psi \frac{\partial \omega}{\partial x} + \varphi \frac{\partial T}{\partial x} \tag{25}$$

$$\frac{\partial w}{\partial y} = \psi \frac{\partial \omega}{\partial y} + \varphi \frac{\partial T}{\partial y} \tag{26}$$

Introducing dimensionless temperature

$$\theta = \frac{T - T_{ci}}{T_{hi} - T_{ci}} \tag{27}$$

and time

$$\tau = \frac{tN}{60} \tag{28}$$

as well as coordinates

$$x^* = \frac{x}{L} \tag{29}$$

$$y^* = \frac{y}{\delta} \tag{30}$$

energy Eq. (6) can be normalized to

$$\frac{\partial \theta}{\partial \tau} = k_x^* \frac{\partial^2 \theta}{\partial x^{*2}} + k_y^* \frac{\partial^2 \theta}{\partial y^{*2}} + q_{st}^* \frac{\partial \omega}{\partial \tau} \tag{31}$$

where

$$k_x^* = \frac{60 k_d}{N L^2 \rho_d (c_{tot} - q_{st}\varphi)} \tag{32}$$

$$k_y^* = \frac{60 k_d}{N \delta^2 \rho_d (c_{tot} - q_{st}\varphi)} \tag{33}$$

$$q_{st}^* = \frac{q_{st}\rho_d \psi}{\rho_d (c_{tot} - q_{st}\varphi)(T_h - T_c)} \tag{34}$$

where N is the rotary speed of the wheel in rpm.

The mass Eq. (8) can be normalized to

$$\frac{\partial \omega}{\partial \tau} + \beta_0^* \frac{\partial \theta}{\partial \tau} = \beta_x \frac{\partial}{\partial x^*}\left(\lambda_\omega \frac{\partial \omega}{\partial x^*} + \lambda_T \frac{\partial \theta}{\partial x^*}\right) + \beta_y \frac{\partial}{\partial y^*}\left(\lambda_\omega \frac{\partial \omega}{\partial y^*} + \lambda_T \frac{\partial \theta}{\partial y^*}\right) \tag{35}$$

where

$$\beta_0^* = \frac{\rho_d \varphi (T_h - T_c)}{\varepsilon_t \rho_a + \psi \rho_d} \tag{36}$$

$$\lambda_\omega = \rho_a D_A + \rho_d D_S \psi \tag{37}$$

$$\lambda_T = \rho_d D_S \varphi (T_h - T_c) \tag{38}$$

$$\beta_x = \frac{60}{NL^2(\varepsilon_t \rho_a + \psi \rho_d)} \tag{39}$$

$$\beta_y = \frac{60}{N\delta^2(\varepsilon_t \rho_a + \psi \rho_d)} \tag{40}$$

Accordingly, the boundary conditions for the solid become

$$\left.\frac{\partial \theta}{\partial y^*}\right|_{y^*=0} = \left.\frac{\partial \theta}{\partial x^*}\right|_{x^*=0} = \left.\frac{\partial \theta}{\partial x^*}\right|_{x^*=1} = 0 \tag{41}$$

$$\left.\frac{\partial \omega}{\partial y^*}\right|_{y^*=0} = \left.\frac{\partial \omega}{\partial x^*}\right|_{x^*=0} = \left.\frac{\partial \omega}{\partial x^*}\right|_{x^*=1} = 0 \tag{42}$$

$$-\left.\frac{\partial \theta}{\partial y^*}\right|_{y^*=1} = Bi(\theta - \theta_g) \tag{43}$$

$$-\left.\frac{\partial \omega}{\partial y^*}\right|_{y^*=1} - \frac{\lambda_T}{\lambda_\omega}\left.\frac{\partial \theta}{\partial y^*}\right|_{y^*=1} = Bi_m(\omega - \omega_g) \tag{44}$$

where Bi is the Biot number for heat transfer

$$Bi = \frac{h\delta}{k_d} \tag{45}$$

and Bi_m is the Biot number for mass transfer

$$Bi_m = \frac{h_m \delta}{\lambda_\omega} \tag{46}$$

The heat and mass transfer equations for the air streams can be normalized as

$$c_1 \frac{\partial \theta_g}{\partial \tau} + \frac{\partial \theta_g}{\partial x^*} = \mathrm{NTU}(\theta_s - \theta_g) \tag{47}$$

$$c_1 \frac{\partial \omega_g}{\partial \tau} + \frac{\partial \omega_g}{\partial x^*} = \mathrm{NTU}_m(\omega_s - \omega_g) \tag{48}$$

where

$$c_1 = \frac{NL}{60u_g} \tag{49}$$

$$\mathrm{NTU} = \frac{hA_s}{\dot{m}_g c_{pg}} \tag{50}$$

$$\mathrm{NTU}_m = \frac{h_m A_s}{\dot{m}_g} \tag{51}$$

where NTU is the commonly recognized number of transfer units, A_s is the total contact area between the air and the solid, $\dot{m}_g$ is the mass flow rate of air stream ($\mathrm{kg\,s^{-1}}$).

2.3. Performance index

If the wheel is used for enthalpy recovery, two effectiveness are defined.

Sensible effectiveness, ε_s

$$\varepsilon_s = \frac{\dot{m}_c(T_{ci} - T_{co})}{\dot{m}_{min}(T_{ci} - T_{hi})} \tag{52}$$

Latent effectiveness, ε_L

$$\varepsilon_L = \frac{\dot{m}_c(\omega_{ci} - \omega_{co})}{\dot{m}_{min}(\omega_{ci} - \omega_{hi})} \tag{53}$$

where $\dot{m}_{min}$ is the least value of adsorption and regenerative mass flows.

Dehumidification effectiveness, ε_d

$$\varepsilon_d = \frac{\omega_{ci} - \omega_{co}}{\omega_{ci}} \tag{54}$$

Specific dehumidification power on the basis of unit mass of desiccant ($\mathrm{kg\,kg^{-1}\,s^{-1}}$)

$$\mathrm{SDP} = \frac{\dot{m}_c(\omega_{ci} - \omega_{co})}{m_d} \tag{55}$$

Specific area of the wheel

$$A_v = \frac{A_s}{V_w} \tag{56}$$

where V_w is the volume of the wheel. The higher the specific area, the more compact the wheel is.

The pressure drop for the wheel can be written as

$$\Delta P = \left(4\xi_c \frac{L}{d_e} + \xi_L\right) \frac{\rho_a u_g^2}{2} \tag{57}$$

where ξ_c is the friction factor of flow channels, and ξ_L is a local friction coefficient that reflects the entrance and exit losses.

For fully developed laminar flow in sinusoidal channels [14],

$$\xi_c = \frac{11.173}{Re} \tag{58}$$

Eqs. (31), (35), (47) and (48) are the governing equations for heat and mass transfer in the wheel, which are strongly coupled with each other.

3. Results and discussion

The two-dimensional heat and mass transfer equations of the desiccant are numerically solved by means of alternating direction implicit (ADI) method [15]. Because the equations are strongly coupled and non-linear, iterations are necessary to get converged values for each time step. Before numerical analysis can be performed, the physical domain of the problem as well as the equations must be discretized. The whole calculating domain is divided into a number of equal-step discrete elements. Each element is identified as a control volume by a nodal point. The numbers of nodes are: 40 in axial, 5 in thickness, and 120 in time (angle). Two possible applications are studied. For enthalpy recovery, the inlet temperature and humidity are: process air, 35 °C, 0.025 kg kg^{-1}; regenerative air (exhaust), 24 °C, 0.013 kg kg^{-1}. For air dehumidification, inlet properties are: process air, 30 °C, 0.021 kg kg^{-1}; regenerative air, 90 °C, 0.021 kg kg^{-1}. The base properties for the simulated desiccant wheel are listed in Table 1. The desiccant material is silica gel. The geometry of the channels in the wheel is sinusoidal with a width of 4.35 mm and a height of 1.74 mm.

3.1. Performance with rotary speeds

There exists an optimum rotary speed at which the efficiency reaches the climax. When a desiccant wheel rotates much faster than the optimum speed, the adsorption and regeneration

Table 1
Configuration of the desiccant wheel

Symbol	Unit	Value
a	m	11×10^{-10}
C		1.0
D_0	m^2 s^{-1}	1.6×10^{-6}
f		0.75
k	W m^{-1} K^{-1}	0.20
L	m	0.1
m_d	kg	15.0
$\dot{m}_g$	kg s^{-1}	0.4
q_{st}	kJ kg^{-1}	2650
w_{max}	kg kg^{-1}	0.25
α_0		0.50
ρ_d	kg m^{-3}	1129
ξ		2.8
δ	mm	0.1
ε_t		0.70

processes are too short, which results in poor performance. On the other hand, when the rotary speed is lower than the optimum, the adsorption and regenerative processes are too long and wasting more energy in sensible heating/cooling rather than in sorption processes, and therefore are less effective. The variations of performance with rotary speed are plotted in Figs. 2 and 3 for dehumidification and enthalpy recovery purposes, respectively. The wall thickness is 0.2 mm. These figures indicate that the optimum rotary speed for air dehumidification is much lower than those for sensible and latent heat recovery. Air dehumidification is more sensitive to rotary speed than enthalpy recovery is. This is because temperature variations of the wheel during dehumidification processes are larger than during enthalpy recovery processes. Wheels need more time to fluctuate between the necessary temperature amplitude in the first case than in the second.

In the following analysis, the wheels are operated at the optimum speeds.

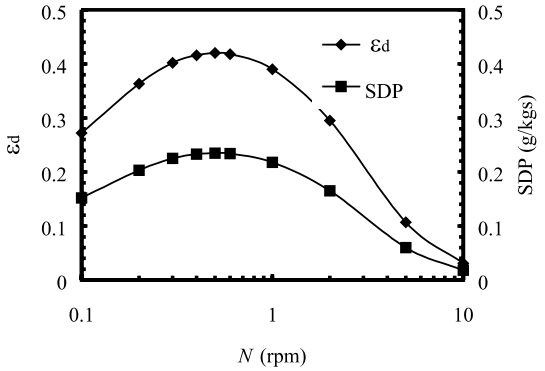

Fig. 2. Performance variations under various rotary speeds with a wall thickness 0.2 mm, for air dehumidification.

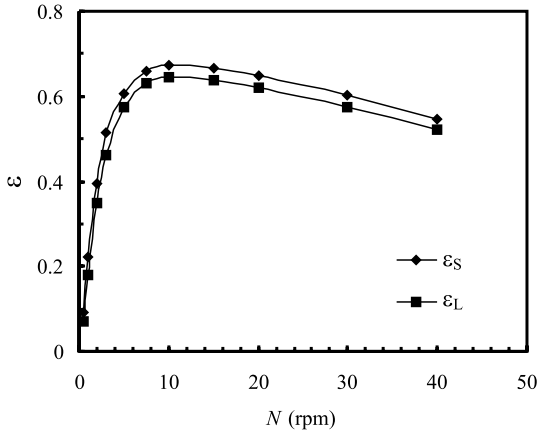

Fig. 3. Performance variations under various rotary speeds with a wall thickness 0.2 mm, for enthalpy recovery.

3.2. Effects of number of transfer units

3.2.1. (a) Various wall thickness

The number of transfer units has a great influence on the system performance. There are many ways to modify NTU. When the wheel mass and channel size are fixed, changing the wall thickness will change the channel numbers, and consequently the contact area and NTU. When the wheel volume and wall thickness are fixed, changing channel sizes will change the number of channels and the packing density, consequently the NTU. Fig. 4 shows the variations of dehumidification effectiveness and specific dehumidification power with increasing NTU through changing wall thickness. When the NTU is in 0–2.5, both the ε_d and the SDP increase rapidly with an increasing NTU, however, when the NTU is bigger than 2.5, a further increase of NTU, i.e., a larger transfer area or a lower mass flow rate, will have little merit in further increasing the performance. These trends are similar to those for a counter-flow sensible heat exchanger. Fig. 5 shows the influence of NTU on enthalpy recovery efficiencies. The NTU of 2.5 is needed for

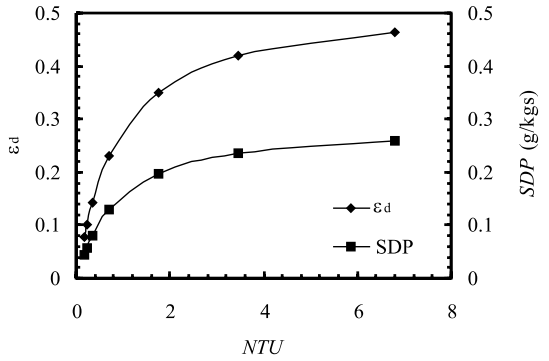

Fig. 4. Effects of NTU on dehumidification performance.

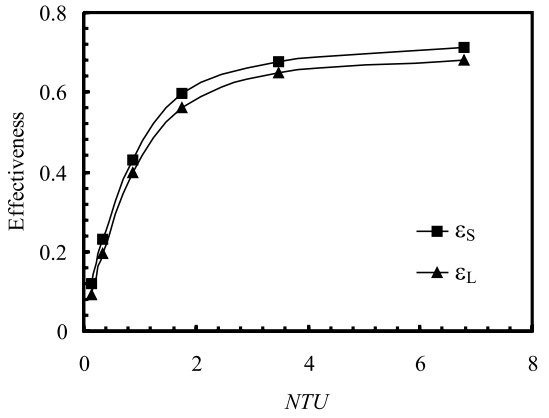

Fig. 5. Effects of NTU on performance for enthalpy recovery.

sensible and latent efficiencies higher than 0.6. It is noted that the latent effectiveness is usually smaller than the sensible effectiveness, because the moisture transfer resistance is usually larger than the heat transfer resistance. In other words, mass diffusion in the solid is far less than the thermal diffusion.

3.2.2. (b) Various A_v

For desiccant wheels, when the total volume of the wheel is fixed, higher specific area can be achieved by constructing with smaller size channels and thinner channel walls. With higher A_v the wheel will be more compact and both the transfer area and the heat mass transfer coefficients will become larger. These factors all contribute to an increased performance, as shown in Fig. 6 for dehumidification and Fig. 7 for enthalpy recovery. As can be seen, the effectiveness rises almost linearly with increasing specific area. Therefore, in practice, the honeycomb-type desiccant wheels which have large contact areas should be recommended. However, increased performance is achieved at the price of increased pressure drop, as shown in Fig. 8. The pressure drop rises rapidly with A_v. In other words, fan power requirement will be increased for honeycomb wheels to

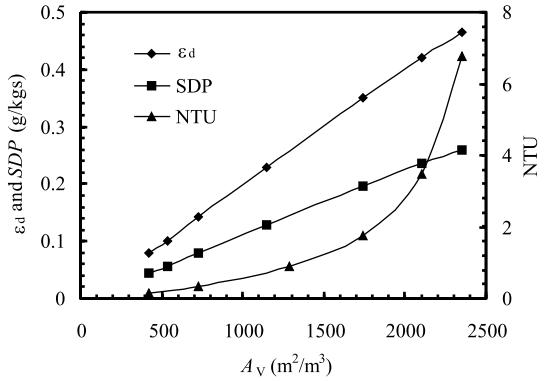

Fig. 6. Effects of specific area on dehumidification performance.

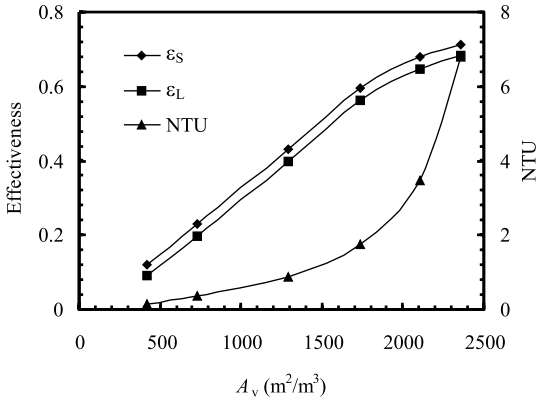

Fig. 7. Effects of specific area on performance for enthalpy recovery.

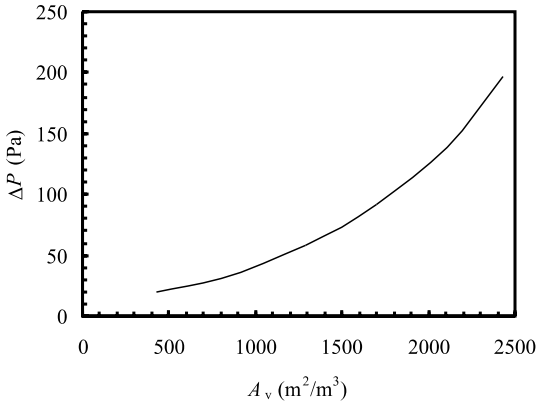

Fig. 8. Pressure drop under various specific area, $\dot{m}_g = 0.4\ \mathrm{kg\,s^{-1}}$, $m_d = 15$ kg.

realize higher performance. Eventually, a compromise between increased A_v and increased pressure drop has to be maintained. It is obvious that NTU increases with A_v.

3.3. Temperature and humidity profiles in the wheel

Temperature and humidity fields in the wheel can be seen from Figs. 9 and 10. Variations of the temperatures (a) and humidities (b) of air inlet and the channel mean are plotted against the wheel angle for dehumidification in Fig. 9 and for enthalpy recovery in Fig. 10 respectively. The values at two local positions in the channel wall (one is near cool air inlet, the other is near warm air inlet) are also plotted in the figures. The coordinates for the two points are: point 1, $x^* = 0.01$, $y^* = 0.5$; point 2, $x^* = 0.99$, $y^* = 0.5$.

From Fig. 9, it can be seen that in dehumidification, desiccant near the warm air inlet has a larger temperature wave than that near the cool air inlet, but the amplitudes of humidity waves are almost the same at these two positions. The mean temperatures at positions near the warm air inlet are higher than those neat the cool air inlet. However, the mean humidities near the warm air inlet are lower than those near the cool air inlet. These facts reveal that the higher the temperature, the lower the humidity ratio for desiccant. During the heating period, the mean humidity of desiccant is higher than that of the air inlet, causing moisture to be desorbed from desiccant to air; while during the cooling period, the mean humidity of desiccant is lower than that of air inlet, causing moisture to be adsorbed from the air to the desiccant.

From Fig. 10, it is seen that during cooling period, humidities in desiccant (both local and mean) are higher than those in air stream and moisture desorbs from the desiccant to the cooling air, while during the heating period, humidities in desiccant are lower than those in air stream and moisture adsorbs from the air to the desiccant. These phenomena in enthalpy recovery are just opposite to those in air dehumidification. Furthermore, the amplitudes of temperature and humidity waves at different locations are not in much disparity, which discloses a fact that temperature and humidity fields in the wheel are more homogeneous in enthalpy recovery than those in dehumidification.

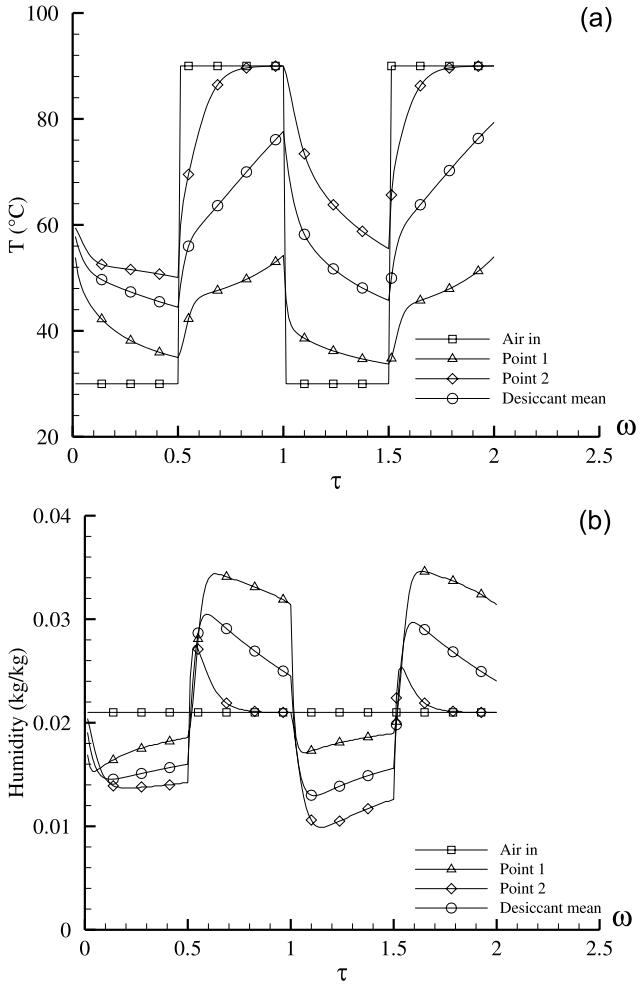

Fig. 9. Variations of the temperature (a) and humidity (b) of two local points, wheel mean and air inlet across the wheel angle for dehumidification. Point 1: near inlet; point 2: near outlet.

3.4. Cycles in psychrometric charts

The cycle the desiccant undergoes during a revolving is certainly of interest. The evolutions of the states of desiccant mean and air outlet in relation to wheel angle are plotted in psychrometric charts, as shown in Fig. 11 for dehumidification and Fig. 12 for enthalpy recovery. In the two figures, the dashed lines are constant enthalpy lines and the inlet states of air streams are represented by points Hi for warm air and Ci for cool air. The arrows indicate the directions of angle increasing or wheel revolving. Points Ho and Co represent the two average outlet air states for heating stream and cooling stream respectively. For the desiccant, three properties, namely, water content, air humidity in the pores, and temperature, are plotted in the graph simultaneously.

Let us first see the cycles in air dehumidification. Fig. 11(a) shows the variations of desiccant mean humidity and water uptake with temperature in a cycle. Here the mean values of desiccant

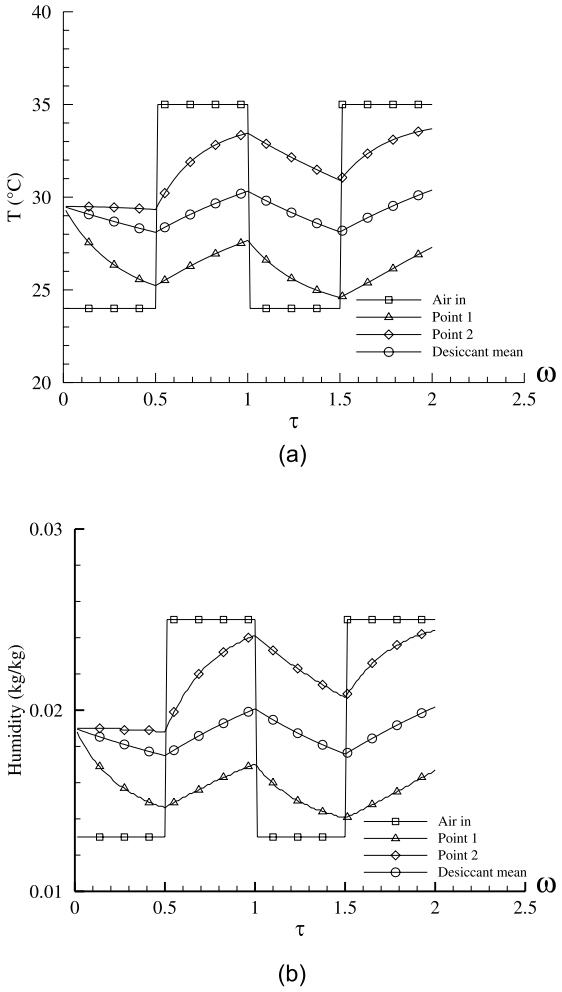

Fig. 10. Variations of the temperature (a) and humidity (b) of two local points, wheel mean and air inlet across the wheel angle for enthalpy recovery. Point 1: near inlet; point 2: near outlet.

are calculated across a channel. Fig. 11(b) shows evolutions of the humidity and temperature of the outlet air stream. The whole cycle for the desiccant at a fixed position comprises two processes:

Process *abc*: This is the dehumidification process for the cool air whose inlet state is point Ci. The outlet states of the air stream across wheel angle lie on the line *abc* whose average is denoted by Co. Therefore the average process for cool air is the thick line Ci → Co. The two figures show that the desiccant temperature drops continuously and the water uptake rises steadily as the wheel revolves. However, the humidity variations are more complicated. From *a* to *b*, the humidities in both the desiccant and the outlet air drop quickly to their lowest values. This period is very short (1/5 of *abc*) and the water content in desiccant changes very little, so it is called isosteric cooling period. However, desiccant temperature decreases substantially in this period, which causes humidities to drop sharply based on sorption isotherms. The heat transferred in this phase is mainly

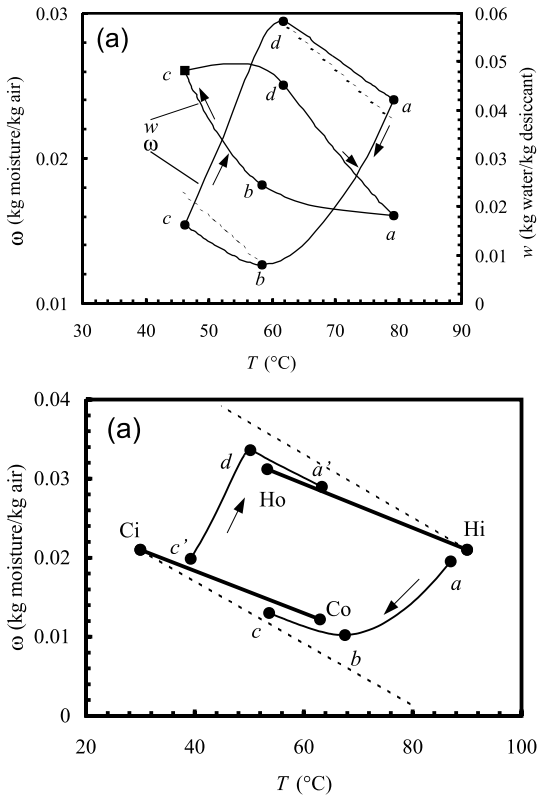

Fig. 11. Variations of the states of desiccant mean (a) and outlet air (b) during wheel revolving for dehumidification: *abc*, during dehumidification; *cda* or *c′da′*, during heating, dashed lines: constant enthalpy.

sensible heat due to the fact that little moisture is adsorbed. From *b* to *c*, the humidities in the desiccant and the outlet air go up slowly from the lowest values. In this period, a large amount of moisture is adsorbed by desiccant and therefore it is called adsorption period. Heat transferred in this phase is mainly sorption heat. Since the desiccant goes toward saturation with increasing quantities of moisture being adsorbed, humidities in desiccant and air stream rise continuously.

Process *cda* (*c′da′* for air): This is the re-activation period for the desiccant with a warm air stream whose inlet state is point Hi and whose mean outlet state is Ho. The outlet states of air distributed along line *c′da′*, depending on the wheel angle. From *c* to *d* (*c′* to *d* for air), this is the isosteric heating phase during which desiccant temperature rises swiftly with water uptake slightly changed. The humidities in the desiccant go up quickly for the preparation of moisture desorption. From *d* to *a* (*d* to *a′* for air), this is the desorption phase during which a large quantities of moisture desorbs from desiccant to air stream. Since the desiccant has less and less water, the humidities decrease with wheel revolving. As in the isosteric cooling process, heat transferred in the isosteric heating phase is mainly sensible heat, while in the desorption phase heat is mainly sorption heat.

During adsorption process for air Ci → Co, enthalpy increases and during re-activation process Hi → Ho, enthalpy decreases for air stream. However, from the point of view of wheel angle,

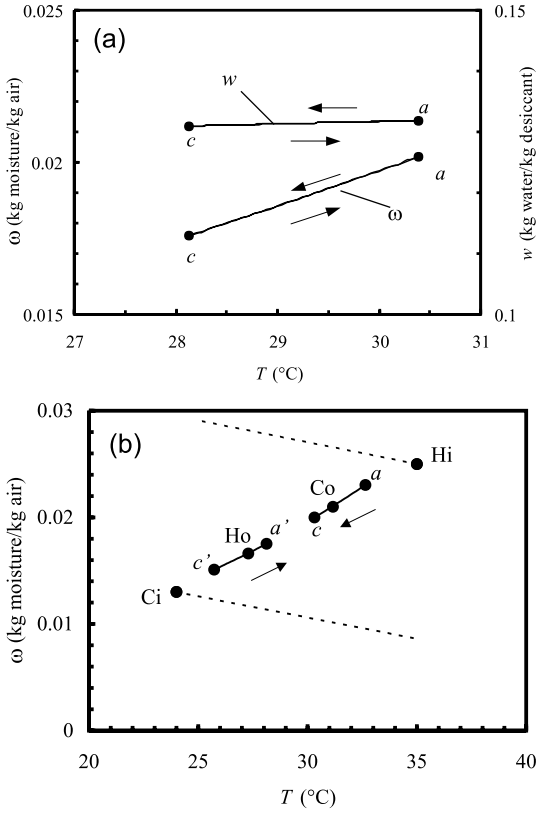

Fig. 12. Variations of the states of desiccant mean (a) and outlet air (b) during wheel revolving for enthalpy recovery: *ac*, during cooling; *ca* or $c'a'$, during heating; dashed lines: constant enthalpy.

during process *abc*, enthalpy of outlet air decreases, and during process $c'da'$, enthalpy of outlet air increases with increasing angle. Furthermore, most of the enthalpy decrease/increase occurs in *ab* and $c'd$ sections. Processes *bc* and da' are almost parallel to constant enthalpy lines. This proves that ideal adsorption and desorption processes are constant enthalpy processes. It is the isosteric heating and cooling processes that makes the real processes in desiccant wheels non-constant enthalpy. In other words, sensible heat leads to the deviation of adsorption/desorption processes from constant enthalpy lines. It is also observed that outlet air states move toward constant enthalpy lines that go through air inlet states with wheel revolving (angle increasing), i.e., processes will become more and more constant enthalpy with wheel revolving.

Fig. 12 shows the variations of the states of desiccant mean and outlet air with respect to wheel revolving for enthalpy recovery. The desiccant mean states evolve along the same line (*ac*) during the cooling process as during the heating process (*ca*), but with an opposite direction. The outlet states of air distribute along line *ac* for cooling process whose inlet is Ci and mean outlet is Co, and along line $c'a'$ for the heating process, where the inlet is Hi and the mean outlet is Ho, respectively. The two inlet states Hi and Ci are on the same line of *ac* or $c'a'$. During heating, both the temperature and the humidity increase, while during cooling, both the temperature and the

humidity decrease with wheel revolving. As a result, enthalpy increases for Ci → Co (cooling air inlet to outlet) and decreases for Hi → Ho (heating air inlet to outlet). The variation of water uptake in desiccant during a wheel working cycle is relatively very small. This is the reason why wheels for enthalpy recovery applications should be rotated much faster than those for dehumidification to realize optimized performances.

4. Conclusions

The two-dimensional, dual-diffusion transient heat and mass transfer model presented in this study is superior to other one-dimensional ones. The advantages of such a model lie in the fact that it considers the heat conduction, the surface and gaseous diffusion in both the axial and the thickness directions simultaneously. The effects of the channel wall thickness can be investigated. Many other structural and operating parameters of the wheel could also be studied.

The results indicate that the optimum rotary speed for air dehumidification is much lower than that for enthalpy recovery. In both cases, honeycomb-type wheels are recommended since a thick channel wall is harmful to the heat mass transfers in the solid. An NTU of 2.5 is needed for desiccant wheels to have a good performance. The wheel for enthalpy recovery has more homogeneous temperature and humidity fields than a wheel for dehumidification. In dehumidification, desiccant near the warm air inlet has a larger temperature wave than that near the cool air inlet, but the amplitudes of humidity waves are almost the same at these two positions. Cycles in psychrometric charts show that for air dehumidification, there are distinct four phases, i.e., isosteric heating, desorption, isosteric cooling and adsorption. However, for enthalpy recovery, the heating and the cooling processes can be represented by a single straight line, but in opposite directions.

Acknowledgements

This research is funded by the postdoctoral fellowship of the Hong Kong Polytechnic University.

References

[1] A. Kodama, M. Goto, T. Hirose, T. Kuma, Experimental study of optimal operation for a honeycomb adsorber operated with thermal swing, Journal of Chemical Engineering of Japan 26 (1993) 530–535.
[2] R. Tauscher, U. Dinglreiter, B. Durst, F. Mayinger, Transport processes in narrow channels with application to rotary exchangers, Heat and Mass Transfer 35 (1999) 123–131.
[3] W. Zheng, W.M. Worek, Numerical simulation of combined heat and mass transfer processes in a rotary dehumidifier, Numerical Heat Transfer, part A: Applications 23 (1993) 211–232.
[4] W. Zheng, W.M. Worek, D. Novolsel, Effect of operating conditions on optimal performance of rotary dehumidifiers, ASME Journal of Energy Resources Technology 117 (1995) 62–66.
[5] J.Y. San, S.C. Hsiau, Effect of axial solid heat conduction and mass diffusion in a rotary heat and mass regenerator, International Journal of Heat and Mass Transfer 36 (1993) 2051–2059.

[6] C.J. Simonson, R.W. Besant, Heat and moisture transfer in energy wheels during sorption, condensation, and frosting conditions, ASME Journal of Heat and Transfer 120 (1998) 699–708.
[7] C.J. Simonson, R.W. Besant, Energy wheel effectiveness: part I—development of dimensionless groups, International Journal of Heat and Mass Transfer 42 (1999) 2161–2170.
[8] J.J. Jurinak, J.W. Mitchell, Effect of matrix properties on the performance of a counterflow rotary dehumidifier, ASME Journal of Heat Transfer 106 (1984) 638–645.
[9] W. Zheng, W.M. Worek, Numerical simulation of combined heat and mass transfer processes in a rotary dehumidifier, Numerical Heat Transfer, part A: Applications 23 (1993) 211–232.
[10] J.Y. San, S.C. Hsiau, Effect of axial solid heat conduction and mass diffusion in a rotary heat and mass regenerator, International Journal of Heat and Mass Transfer 36 (1993) 2051–2059.
[11] C.J. Simonson, R.W. Besant, Heat and moisture transfer in energy wheels during sorption, condensation, and frosting conditions, ASME Journal of Heat Transfer 120 (1998) 699–708.
[12] A.A. Pesaran, A.F. Mills, Moisture transport in silica gel packed beds. I—theoretical study, International Journal of Heat and Mass Transfer 30 (1987) 1037–1049.
[13] P. Majumdar, Heat and mass transfer in composite desiccant pore structures for dehumidification, Solar Energy 62 (1998) 1–10.
[14] L.Z. Zhang, J.L. Niu, A Numerical study of laminar forced convection in sinusoidal ducts with arc lower boundaries under uniform wall temperature, Numerical Heat Transfer, part A: Applications 40 (2001) 55–72.
[15] A.A. Samarskii, P.N. Vabishchevich, Computational Heat Transfer, John Wiley & Sons Inc., New York, 1995.